Drying and Film Formation of Industrial Waterborne Latices

I. Ludwig, W. Schabel and M. Kind
Universität Karlsruhe (TH), 76128 Karlsruhe, Germany

J.-C. Castaing and P. Ferlin
Rhodia Recherches et Technologies, Aubervilliers, France

DOI 10.1002/aic.11098
Published online January 19, 2006 in Wiley InterScience (www.interscience.wiley.com).

Experimental evidence is given for the mechanism of film formation from industrial waterborne latices using Inverse-Micro-Raman-Spectroscopy (IMRS). In the vertical direction of the film drying is gas-side controlled, indicated by uniform water concentration profiles. In the horizontal direction inhomogeneous drying resulting from a horizontal mass flux toward the edge of the film and the formation of a drying front are observed. The completeness of film formation is tested by so-called IMRS redispersion experiments. For hard latices ($T_{experiment} \simeq T_{mff}$) particle deformation is incomplete and the final coating—although transparent and optically clear—is a porous structure with a network of surfactant material located at the particle interfaces. The use of a film-forming aid lowers the polymer's minimum film formation temperature (T_{mff}) and facilitates particle deformation and polymer interdiffusion. The result is a nonporous film structure where individual particles and a network of surfactant material are no longer observed. IMRS redispersion experiments are compared with pictures of the final coating surface obtained from atomic force microscopy (AFM). © 2007 American Institute of Chemical Engineers *AIChE J,* 53: 549–560, 2007

Keywords: water-based coatings, latex, drying, film formation, Raman spectroscopy

Introduction

As a result of stricter environmental regulations, aqueous latex dispersions, among others such as aqueous polyurethane dispersions or alkyd emulsions, are considered to constitute one alternative for future coatings and paints compared to solvent-based formulations. Industry invests significant time and effort into the development of water-based systems that show a drying behavior comparable to that of the established solvent-based formulations. Further improvements in the application properties of water-based formulations require a fundamental understanding of the drying and film formation mechanism from colloidal dispersions.

During the last decades many researchers have dealt with the question of latex film formation,[1–3] revealing that film formation from aqueous latex dispersions is very complex. Experimental studies on a broad variety of latex dispersions prepared and dried under many different conditions and conducted by a large number of different methods have led to a flood of information containing valuable details of latex film formation but that are often not transferable even to closely related systems.

A large number of experimental techniques have been used to investigate different aspects of spacing and deformation of the latex particles: Structural changes in films cast from soft particles protected by hydrophilic membranes have been extensively studied by small-angle neutron scattering (SANS).[4–7] The same technique has also been applied to study particle coalescence and surfactant

desorption during film formation from carboxylated acrylic latices.[8] The use of transmission spectrophotometry has been reported to follow variations in interparticle distance and displacement during the film formation of acrylic latices.[9]

The impact of functional groups at the surface of acrylic latex particles on the kinetics of polymer interdiffusion has been investigated by fluorescence decay measurements.[10] Attenuated total reflectance (ATR) Fourier transform infrared (FTIR) spectroscopy has been used for the study of surfactant–latex molecular level interactions[11] and the distribution of surfactant in the final latex film.[12] Dynamic mechanical analysis has also proved to be a useful option in the study of polymer interdiffusion.[13]

Microscopic techniques have been applied to characterize deformation and coalescence of particles at the film surface. High-resolution cryogenic scanning electron microscopy (CSEM) has been used to investigate microstructure development during drying of monodisperse and bimodal latex coatings.[14] Information about the surface morphology of waterborne pressure-sensitive adhesives manufactured from acrylic ester copolymers has been obtained using tapping-mode atomic force microscopy.[15]

To our knowledge, confocal Raman spectroscopy has been applied to the field of latex film drying only to investigate the distribution of water-soluble and surface-active species in acrylic latex films.[16,17]

Obviously, the major part of the existing experimental data deals with aspects of particle ordering and deformation during latex film formation. Although there is fundamental interest in the role of water during drying, experimental data dealing with this aspect are rare. Apparently, this arises from a lack of experimental methods, which can detect water and which have a space and time resolution required to follow local water concentration in the film.

The investigation of film drying by means of gravimetric measurements at defined conditions is state of the art.[18] Currently, we are aware of only the two following experimental studies dealing with water distribution in latex films. Solid-state nuclear magnetic resonance (NMR) spectroscopy has been used to investigate the influence of different amounts of surfactant on the homogeneity of the vertical drying process of thick films (~5 mm).[19] Excellent data have been obtained from magnetic resonance (MR) profiling used to monitor vertical water concentration profiles in thin films (~300 μm) of alkyd emulsions[20] and also to measure horizontal water concentration profiles resulting from inhomogeneous drying within a drop of latex dispersion.[21]

In this work we present the use of Inverse Micro-Raman Spectroscopy (IMRS) to obtain quantitative water concentration profiles in thin acrylic latex films during drying in both the vertical and the horizontal directions. To our knowledge, the IMRS data show an optical and time resolution not yet presented by others. Besides investigation of drying, IMRS is used to monitor water diffusion into dry latex films. In combination with atomic force microscopy (AFM) we obtain information about the dry film structure.

Taken together, the data will give insight into many different aspects of latex film drying and film formation. Important findings reported by others can be supported by our experimental data.

Latex Film Formation

Different theories have been proposed regarding the film-formation process and the forces responsible for film formation. Review articles on this topic can be found in the literature.[1–3] Brown[22] claims that particle coalescence occurs when the forces that favor film formation, such as capillary forces and van der Waals forces, are greater than the repulsive forces, such as electrostatic repulsion and resistance against deformation. Dillon[23] states that drying and particle coalescence occur separately and that dry sintering of the latex particles is attributed to the interfacial tension of particles and air. Sheetz[24] describes film formation as a process where an osmotic pressure difference, caused by a dry skin layer on top of the wet polymer film, is responsible for particle deformation and coalescence.

Depending on the experimental conditions and the material's properties, experimental data have been reported that prove the importance of any of the above-mentioned driving forces for film formation. A recently developed model predicts the conditions necessary for the different driving forces to be dominant during film formation.[25]

Conventional understanding is that the process of film formation can be described by a mechanism that includes four consecutive stages: (1) the concentration of the latex dispersion; (2) particle contact; (3) particle deformation; and (4) the interdiffusion of the polymer chains across the particle boundaries, which is necessary to form a mechanically stable film. In Figure 1, the different stages of film formation are illustrated. In the initial dispersion the latex particles are stabilized by a large amount of surfactant adsorbed at the particle surface. Phase (1) of the film-formation process is characterized by a constant loss of water with time. The concentration of latex particles continually increases and—depending on the drying

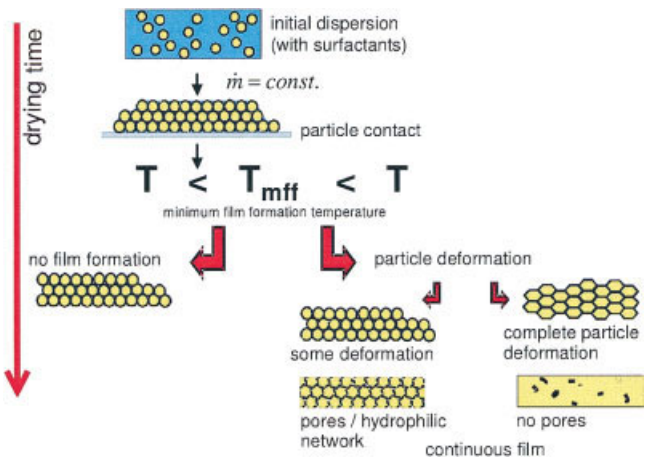

Figure 1. The general mechanism of latex film formation.

Water evaporates at a constant rate until the latex particles come into contact and form an ordered structure. Film formation takes place only above a minimum film formation temperature (T_{mff}). Then, the latex particles will deform as a result of surface tension and capillary forces. Complete particle deformation will occur only well above T_{mff}. The final film properties are obtained long after water has been removed from the film. [Color figure can be viewed in the online issue, which is available at www.interscience.wiley.com]

conditions, the nature and strength of particle stabilization, and the ionic strength of the serum—the particles come into close contact and pack in a more or less ordered way. The closest possible packing of monodisperse spheres [face-centered cubic (fcc)] has a volume fraction of polymer particles of $\Phi = 0.74$, which corresponds to a water content of $X \simeq 0.35$ g water/g polymer. Phase (2) of the model starts where the undeformed particles first come into contact. At this point, phase (3)—significant particle deformation—can take place only if drying occurs at temperatures well above a so-called minimum film formation temperature (T_{mff}). By definition this is the drying temperature above which a transparent and crack-free polymer film will form. For complete film formation without pores, spherical particles have to deform into rhombic dodecahedrons. In phase (4) the film properties are fully obtained long after water has been removed from the film. Here, the polymer chain mobility, which controls coalescence, depends on the difference between the drying temperature and the polymer's glass-transition temperature (T_g).

If drying temperatures are close to T_{mff}, particle deformation will be incomplete. Although the final film will be transparent, it is a porous structure of individual particles with a network of hydrophilic surfactant material present at the particle–particle interface. The extent of particle deformation dependent on T_{mff} has been studied using turbidity measurements.[9] According to some authors[2–5] the rupture of the surfactant layer, separating the deformed latex particles, is prerequisite to encouraging polymer interdiffusion and developing mechanical strength.[26] For drying well above T_{mff} particle deformation and polymer diffusion will be sufficiently strong to destroy the network of hydrophilic surfactant material to form a nonporous film.

Measurement Techniques

A measurement technique—Inverse Micro-Raman Spectroscopy (IMRS)—has been developed at Karlsruhe University (TH) in collaboration with a spectrometer company[27] by combining an inverse microscope with a confocal Raman spectrometer (Figure 2). With IMRS, the local water content within thin latex films can be obtained quantitatively during drying with an optical resolution of 2–3 μm and a time resolution of about 1 s. The method includes the preparation of a sample film within the drying channel and subsequent drying at defined conditions. As shown in Figure 2, a laser beam is focused into the latex film by a system of mirrors and optical lenses. Within the film, a small part of the light is scattered—elastically or inelastically—as a result of the interaction of the laser beam with the molecules of the sample. Only the inelastically scattered light—the Raman light—can pass back through the interference pattern of the notch filter. High spatial resolution is achieved by the confocal pinhole, which is optically coupled with the objective's focus. It allows only backscattered light from the plane of focus to be detected by the spectrometer.

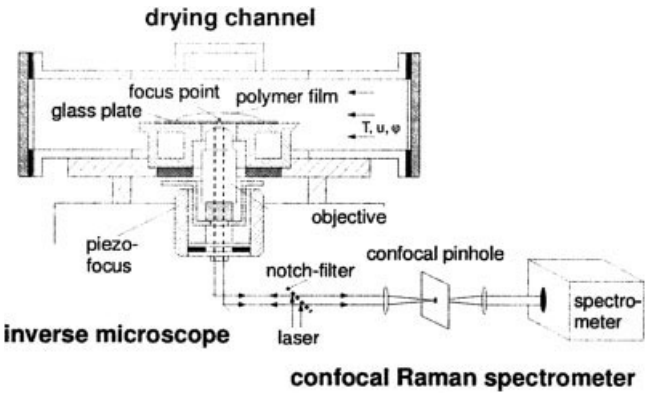

Figure 2. Inverse-Micro-Raman Spectroscopy (IMRS).

Within the drying channel, a latex film dries at defined conditions. The laser beam is focused into the sample and the inelastically scattered light from the plane of focus, the Raman light, is detected by the spectrometer. The signal gives quantitative information about the water content within the film during drying.

The technique is well suited to investigate the drying mechanism of both solvent-based polymer solutions[28] and water-based dispersions.

Quantitative Data Evaluation in Scattering Media (such as Latex Dispersions)

The peaks of the Raman spectrum are characteristic for the different components of the sample under investigation. A method for calibration and quantitative evaluation of Raman data from solvent-based polymer solutions is given in the literature[28,29] using the intensity ratio of solvent and polymer peak. The Raman signal of a chemical species is linear proportional to its concentration and depends on a number of specific and experimental factors:

$$I_i = \underbrace{c_i \frac{\partial \sigma_i}{\partial \Omega} \tilde{M}_i^{-1}}_{\text{specific}} \underbrace{I_0 N_A V C F^{-1} \Omega_{obs}}_{\text{experimental}} \tag{1}$$

Because of the linear relationship between intensity and concentration the ratio of solvent (i) and polymer (p) peak intensity results in the following simple equation, where all experimental factors can be neglected. The constant $K_{i,p}$ can be obtained from calibration measurements of samples of known concentration:

$$\frac{I_i}{I_P} = \left(\frac{c_i}{c_P}\right) \underbrace{\left(\frac{\partial \sigma_i / \partial \Omega \, \tilde{M}_i^{-1}}{\partial \sigma_P / \partial \Omega \, \tilde{M}_P^{-1}}\right)}_{K_{i,p}} \underbrace{\left(\frac{I_0 N_A V C F^{-1} \Omega_{obs}}{I_0 N_A V C F^{-1} \Omega_{obs}}\right)}_{=1} \tag{2}$$

The evaluation method valid for solvent-based systems can also be used to obtain concentration profiles within water-based latex dispersions, despite the observed loss of laser light intensity resulting from light scattering at the particles as the laser is focused deeper into the wet film. Figure 3a shows a three-dimensional profile of the wet latex film created by Raman spectra at different positions of the film. The decrease of signal intensity toward the film surface, indicated by the arrow in Figure 3a, is the result of light scattering. As long as the intensity loss is not wavenumber dependent, light scattering has no impact on the quantitative data evaluation. Figure 3b shows that the intensity ratio of different polymer peaks is constant independent of where in the film the Raman spectrum is taken. This proves that no wavenumber dependency of scattering exists and that a quantitative evaluation using Eq. 2 is therefore still possible. Changes in the

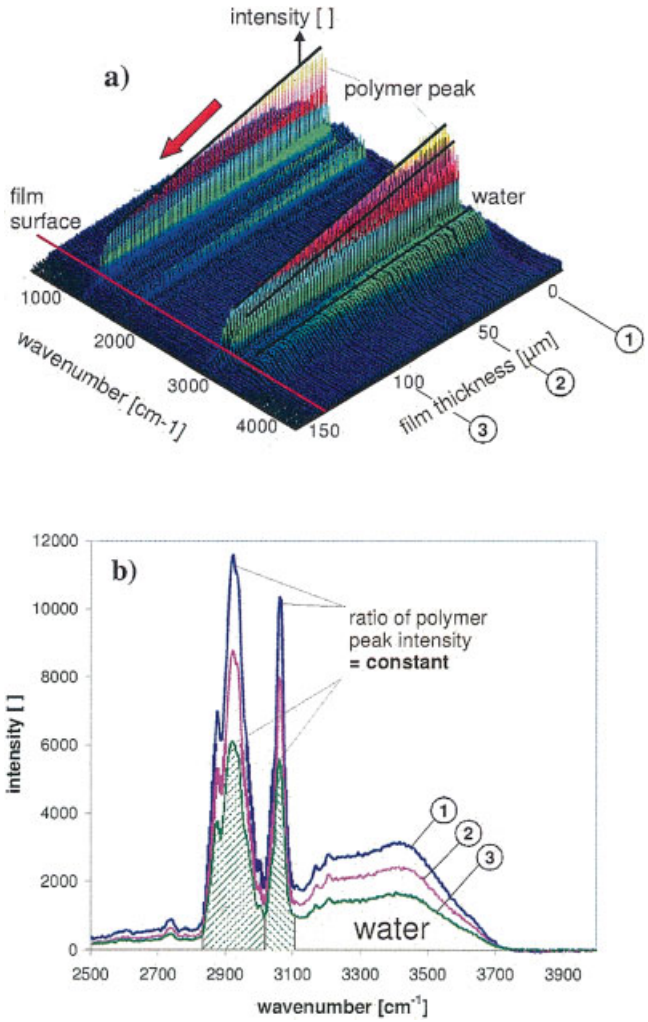

Figure 3. (a) Raman spectra in a wet latex film obtained with the IMRS technique. The decrease of signal intensity resulting from light scattering is highlighted by the arrow. (b) Raman spectra taken at different positions 1, 2, and 3 in the wet latex film. As long as the ratio of polymer peak intensities is constant, independent of where in the film the spectrum is taken, a quantitative evaluation of the data is possible using the above-described method.

[Color figure can be viewed in the online issue, which is available at www.interscience.wiley.com]

ratio of water and polymer peak arise from evaporation and not from light scattering.

The relative shift of focus position during IMRS measurements resulting from a change of refractive index is taken into account by depth of focus and center of gravity corrections.[30]

Characterization of the Latex Dispersion and Experimental Conditions

The experiments were carried out with a 50 wt % dispersion of acrylic latex particles, stabilized by a large amount of surfactant. Additional functional groups are present at the particle surface. The dispersion was used as supplied without further purification. Photon correlation spectroscopy at pH = 7 gave an average particle diameter of about 100 nm. Measurements at different temperatures gave a minimum film formation temperature of the dispersion of $T_{\mathrm{mff}} = 18^{\circ}\mathrm{C}$. For the redispersion experiments a typical film formation aid (2,2,4-trimethyl-1,3-pentandiol-monoisobutyrat) was used to lower the T_{mff} of the initial dispersion.

The experiments were performed at drying conditions considered typical for paints and coatings ($T = 21^{\circ}\mathrm{C}$, $\varphi = 35\%$, $u = 0.05$ m/s). In this work these conditions will be referred to as standard conditions.

Experimental Results and Modeling of Film Drying in the Film's Vertical Direction

To our knowledge vertical drying of latex films—although of great importance for the application properties of latices—has not been subject to many experimental studies so far. As mentioned earlier, we believe that this is, until today, explained by a lack of suitable experimental techniques.

In a theoretical study Routh and Russel showed that the vertical homogeneity of latex films during drying is controlled by a Peclet number (Pe),[25,31,32] defined as

$$\mathrm{Pe} = \frac{d_{\mathrm{start}} E}{D_0} = \frac{6\pi\mu R_0 d_{\mathrm{start}} \dot{m}_{\mathrm{water}}}{kT\rho_{\mathrm{H_2O}}} \tag{3}$$

which gives the rate of particle convection divided by the rate of particle diffusion. Here μ is the viscosity of the continuous medium, R_0 is the particle radius, d_{start} is the initial film thickness, and $\dot{E}$ is the evaporation rate. D_0 represents the Stokes–Einstein diffusion coefficient for the colloidal particles. For $\mathrm{Pe} \ll 1$ diffusion is strong compared to evaporation and thus uniform vertical distribution is expected; for $\mathrm{Pe} \gg 1$ evaporation is dominant, leading to water concentration profiles within the film. Magnetic resonance (MR) profiling has been used to measure water concentration profiles in the film's vertical direction during drying for different Peclet numbers.[20] The high-quality data show the formation of concentration profiles across the film for $\mathrm{Pe} > 1$. In the same study, the formation of concentration gradients was reported to be independent of Pe for a water volume fraction $\Phi_w < 0.1$.

Figure 4 shows the quantitative evaluation of a film-drying experiment for a film of initial thickness $d = 75$ μm and initial solvent content of $X = 0.88$ g water/g polymer obtained by IMRS. The measurement position is in the middle of the sample film (size of the sample: 40×100 mm^2).

During the experiment the laser focus is moved from the bottom of the film (left side in Figure 4) to the film surface (right side) in steps of 5 μm. One complete scan through the film takes about 30 s. This means that the profiles in Figure 4 were not taken at one point in time but during a time period of several seconds, which explains the slight decrease of water content toward the film surface. The experimental data are represented by the symbols. Unlike film drying of solvent-based films,[29] drying of aqueous latex dispersions at standard conditions is gas-side controlled. The Peclet number for the film-drying experiment presented here is $\mathrm{Pe} = 0.03$.

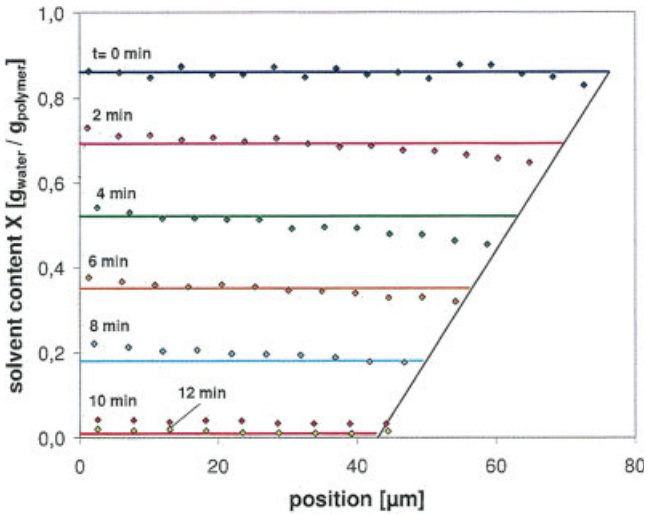

Figure 4. Measured water concentration profiles in the film obtained from IMRS.

The symbols represent the measured water content X vertical across the film; the lines show the calculated values (constant-rate model) . [Color figure can be viewed in the online issue, which is available at www.interscience.wiley.com]

As expected, most of the drying is in the constant rate period (CRP). Down to a water content of $X = 0.05$ g water/g polymer, no concentration gradients form, which would indicate some kind of film-side diffusion resistance. Below this value the drying rate decreases dramatically, a phenomenon also reported by others.[20] In Figure 4, the experimental data are compared to constant-rate model calculations, represented by straight lines. Both model and experiment are in good agreement except for very low water contents.

In the model shown in Figure 5, a simplified Stefan–Maxwell equation is used to describe the mass transfer in the gas phase for single-side diffusion:[33]

$$\dot{m}_{\text{water}} = \tilde{M}_{\text{water}}\,\dot{n}_{\text{water}} = \tilde{M}_{\text{water}}\,\frac{\rho_{\text{gas}}}{\tilde{M}_{\text{air}}}\,\beta_{\text{g,w}}\ln\frac{1-\tilde{y}^{\infty}}{1-\tilde{y}^{*}} \tag{4}$$

This term can also be written as

$$\dot{m}_{\text{water}} = \tilde{M}_{\text{water}}\frac{\rho_{\text{gas}}}{\tilde{M}_{\text{air}}}\,\beta_{\text{g,w}}(\tilde{y}^{*}-\tilde{y}^{\infty})K_{\text{S}} \tag{5}$$

where K_{S}, the Stefan correction term, represents the influence of the overall convective flux on the interaction of the different component fluxes and is defined as

$$K_{\text{S}} = \frac{\ln\frac{1-\tilde{y}^{\infty}}{1-\tilde{y}^{*}}}{\tilde{y}^{*}-\tilde{y}^{\infty}} \tag{6}$$

The molar fraction $\tilde{y}^{*}$ is calculated from Antoine's equation and $\tilde{y}^{\infty}$ is determined by the relative humidity of the process air:

$$\tilde{y}^{\infty} = \frac{p^{*}_{\text{water}}}{p}\,\varphi = \tilde{y}^{*}\varphi \tag{7}$$

The vapor pressure reduction resulting from sorption effects is not taken into account. For our conditions, the Stefan correction term is close to unity ($K_{\text{S}} = 1.02$), which means that the error would be about 2% if the linear approach was used instead of the Stefan–Maxwell equation.

The gas-side mass-transfer coefficient $\beta_{\text{g,w}}$ for water evaporation from the film is calculated using the well-known Sherwood correlation,[34] valid for laminar flow and plate geometry:

$$\text{Sh} = \frac{\beta_{\text{g,w}}L}{\delta_{\text{w}}} = 0.664\sqrt{\text{Re}}(\text{Sc})^{0.33} \tag{8}$$

Here L is the distance between the edge of the film and the measurement position in direction of the airflow. The diffusion coefficient δ_{w} is calculated from the Fuller equation.[35] The calculated values for δ_{w} and $\beta_{\text{g,w}}$ at our standard conditions are δ_{w} ($T = 21^{\circ}$C) $= 2.5 \times 10^{-5}$ m^2/s and $\beta_{\text{g,w}}$ ($T = 21^{\circ}$C) $= 2.3 \times 10^{-3}$ m/s.

Finally, the water content X in the film at time t and the film thickness d can be calculated from

$$X_{i+1} = X_i - \frac{\dot{m}(t_{i+1}-t_i)}{x d_{\text{start}}\rho_{\text{disp,start}}} \tag{9}$$

$$d = \frac{d_{\text{end}}}{\left(1-\frac{\Delta X x \rho_{\text{disp,start}}}{\rho_{\text{H}_2\text{O}}}\right)} \tag{10}$$

where x is the mass fraction of the initial dispersion, $\rho_{\text{disp,start}}$ is the original dispersion density, $\rho_{\text{H}_2\text{O}}$ is the density of water, and d_{start} and d_{end} represent, respectively, the initial and final film thicknesses.

Experimental Results on Inhomogeneous Drying in the Film's Horizontal Direction

With respect to water-based latex formulations, horizontal inhomogeneous drying is the reason for serious application

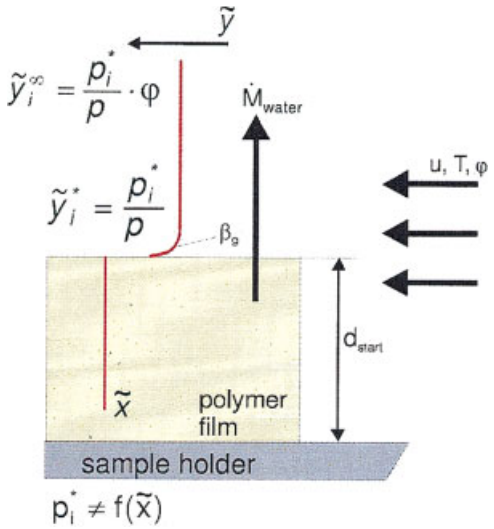

Figure 5. The constant-rate model to describe gas-side controlled film drying.

[Color figure can be viewed in the online issue, which is available at www.interscience.wiley.com]

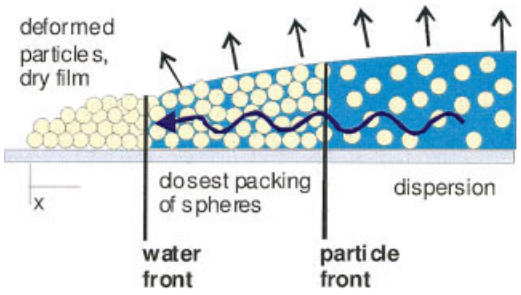

Figure 6. A general representation of the horizontal drying mechanism for finite capillary pressure.

[Color figure can be viewed in the online issue, which is available at www.interscience.wiley.com]

problems, such as lap lines in the final coating. Industry has a fundamental interest in how to influence and avoid lateral inhomogeneous drying.

Two-dimensional ordering of micrometer-size latex spheres on a glass plate investigated by optical microscopy was previously reported in the early 1990s.[36] Particle ordering in the highly diluted dispersion starts as soon as the thickness of the water layer has decreased to the size of the particle diameter. The attractive capillary force resulting from the menisci around the particles is identified as the main driving force for particle ordering and transport of particles toward the ordered regions. Since then, horizontal inhomogeneous drying of latex films, where drying starts at the thinnest point of the film, has often been observed and reported.[1,2] According to the literature, the development of film thickness and solid volume fraction laterally across the film has been modeled by overall momentum and conservation equations: First, the capillary pressure was incorporated into the model as the driving force for horizontal inhomogeneous drying of rigid spheres.[37,39] As a next step particle deformation was included by the viscoelastic deformation of a pair of particles.[38,40] For finite capillary pressure the model considers three different zones: zone I, consisting of a dry zone of deformed particles at the edge; zone II, consisting of closely packed particles; and zone III, consisting of dispersed particles in the center. The zones are separated by a particle and a water front, respectively (Figure 6). Water evaporates from the wet surface area. Horizontal mass flux toward the film edge is caused by the capillary pressure gradient.

Obviously, extensive scientific work has already been done in the field of horizontal inhomogeneous drying of latex films. Nevertheless, experimental data that can be used to evaluate and improve model calculations seem to be rare. A very recent study reports the comparison of horizontal concentration profiles obtained from magnetic resonance experiments with model calculations.[21]

The high-resolution data of film thickness d and solvent content X at different horizontal positions in the film obtained from Inverse-Micro-Raman Spectroscopy can help to validate and further develop model calculations. In the future we plan to study the influence of different additives on inhomogeneous drying of latex films and to compare our experimental data with model calculations. Herein, the first horizontal concentration profiles in thin latex films obtained from

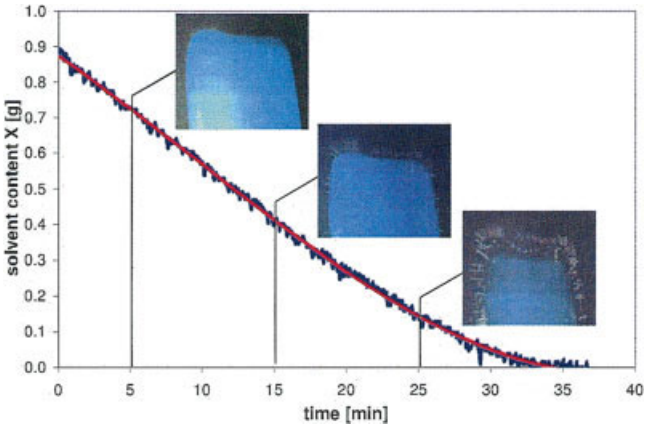

Figure 7. Gravimetric drying curve of a thin latex film. Drying starts at the edge of the film because of a larger evaporation area. A drying front moves toward the center of the film.

[Color figure can be viewed in the online issue, which is available at www.interscience.wiley.com]

IMRS drying experiments are presented. Our findings concerning particle ordering and lateral water transport are in accordance with the results previously reported by others.[36]

An illustration of lateral inhomogeneous drying is given in Figure 7, which shows the gravimetric drying curve of a thin acrylic latex film. From the pictures the formation and motion of the drying front are visible.

For the data acquisition using IMRS, the film is covered by a lid every 2 min throughout drying (Figure 8). This considerably slows down drying and allows measurements at different positions during one acquisition time. Data evaluation gives the water profiles in both vertical and horizontal directions and the film thickness with high accuracy. The distance between two measurement positions in the horizontal direction is 3 mm.

In the freshly applied film, the water content at the different measurement positions is uniform (Figure 9). At the

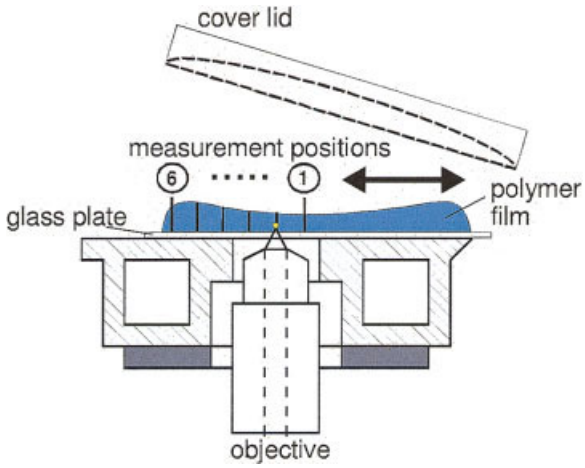

Figure 8. Experimental setup for the investigation of horizontal inhomogeneous film drying.

[Color figure can be viewed in the online issue, which is available at www.interscience.wiley.com]

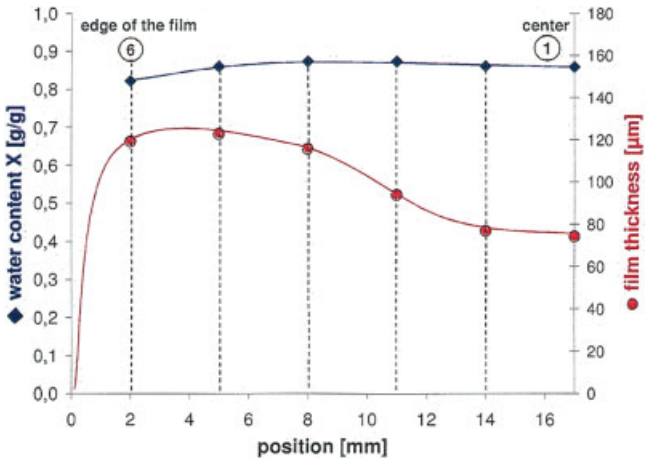

Figure 9. Water content *X* and film thickness *d* at *t* = 0 min.

The symbols represent the values obtained from IMRS measurements; the lines are intended only to guide the eye. Special attention has to be paid to the length scale. [Color figure can be viewed in the online issue, which is available at www.interscience.wiley.com]

same time the initial film thickness is not homogeneous, with the edge being considerably thicker than the center of the film. This is explained by the bad wetting behavior of water-based formulations on glass. The lines in Figure 9 are intended only to guide the eye.

The average initial water content in the film is $X = 0.88$ g water/g polymer, which corresponds to a solid content of roughly 55 mass % polymer (Figure 10). Drying at the edge of the film is faster because of a greater evaporation area and reduced film thickness. This leads to a faster decrease of water content at position 6. At the center (positions 1 and 2) the water content decreases faster as a result of the initial profile of the film having a lower thickness at the center region. Assuming face-centered cubic (fcc) packing of monodisperse spheres, particle contact takes place at a water content of $X = 0.35$ g water/g polymer, represented by the straight line in Figure 10. A remarkable decrease in water content X is observed at the beginning of drying for the edge of the film and toward the end of drying for positions 4 and 5, indicated by the arrows in Figure 10. Faster drying of the edge is also presented in Figure 11, which shows the drying curves (= average water content in vertical direction of the film vs. drying time) obtained at the different positions. A difference in the initial drying rate of position 1 compared to that of position 4 is caused by the nonuniform film thickness. Comparison with Figure 12 shows that the substantial decrease in water content X corresponds to a substantial decrease in film thickness.

The initial steep decrease in water content and film thickness at position 6 can be explained by the formation of menisci between the packed latex spheres at the edge of the film causing a pressure gradient and leading to particle deformation and horizontal mass flux of water and particles toward the film edge. At this point, the distance over which capillary suction is effective is also insufficient to be observed at position 5.

Brown[22] analytically calculated the capillary pressure of a triangular pore of three neighboring particles:

$$p_c = \frac{12.9\gamma}{r_{\text{pore}}} \tag{11}$$

which is dependent on the water–air surface tension γ and the pore radius r_{pore}. If throughout the experiment capillary

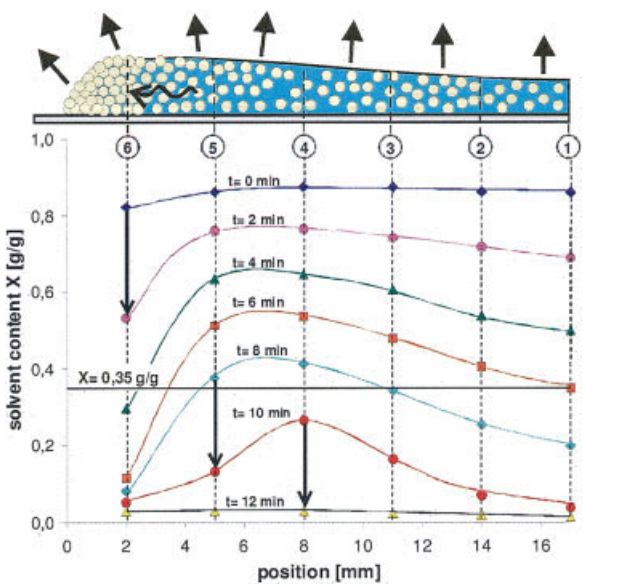

Figure 10. Horizontal concentration profiles in the film during drying.

The initial water content is uniform throughout the film. Drying is faster at the edge caused by a greater evaporation area. The water content at the center decreases faster as a result of the initial profile of the film having a lower thickness at the center region. The lines are intended only to guide the eye. [Color figure can be viewed in the online issue, which is available at www.interscience.wiley.com]

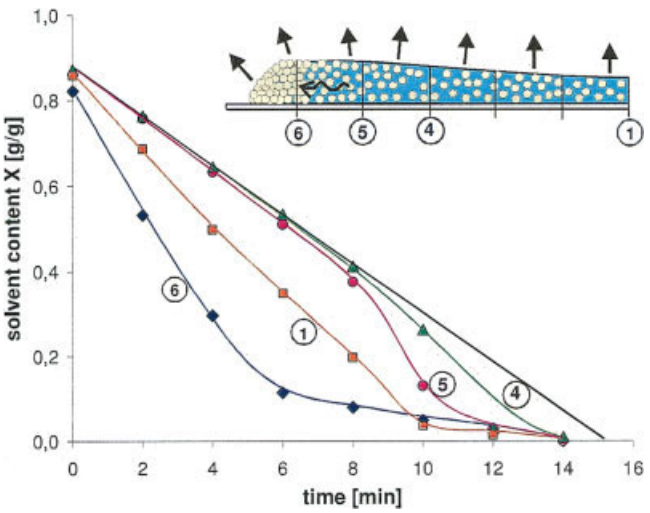

Figure 11. Drying curves at the different positions across the film.

The lines are intended only to guide the eye. [Color figure can be viewed in the online issue, which is available at www.interscience.wiley.com]

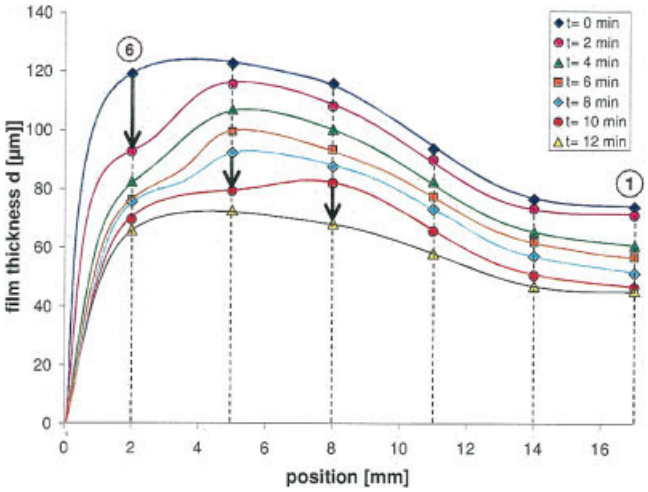

Figure 12. Change in film thickness during drying.

The film is thicker at the edge because of the bad wetting behavior of water-based formulations on glass. The lines are intended only to guide the eye. [Color figure can be viewed in the online issue, which is available at www.interscience.wiley.com]

suction is no longer strong enough to keep the water at the film surface, a water front forms and moves toward the center of the film.

After a drying time of $t = 8$ min a pronounced decrease of water content—indicated by the arrow in Figure 10—is observed at position 5. Combined with an almost dry edge of the film (Figure 10, position 6) and a steep decrease in film thickness, this can be attributed to the drying front moving toward the center of the film. Because at $t = 8$ min the water content has already decreased to a value below the one for fcc packing of spheres the decrease in film thickness must be attributed to particle deformation. After $t = 10$ min the same decrease in water content is observed at the next position closer to the center (position 4).

A representation of the total mass flux (= evaporative flux and horizontal flux) at the different positions in the film is given in Figure 13, which supports the findings described earlier. The flux is calculated from experimental data according to

$$\dot{m}_{\text{water}} = -\rho_{\text{polymer}}\, d_{\text{film,end}}\, \frac{dX}{dt} \tag{12}$$

where ρ_{polymer} is the polymer density, $d_{\text{film,end}}$ is the final film thickness of the dry film, and X is the water content of the film during drying.

The higher flux at the edge of the film (position 6) is a combination of the evaporative flux and the horizontal flux of water and particles, driven by capillary pressure. Figure 13a shows that at the beginning of drying the horizontal flow is spatially limited to the edge of the film. For the rest of the film, drying is at a constant rate during the first 5 min of drying. During this time, water is kept at the edge of the film by capillary suction. As soon as the capillary pressure difference is no longer sufficient, a water front recedes into the film and toward the center. This is indicated by the increased mass flux at positions 4 and 5 for a drying time of $t = 9$ min and $t = 11$ min, respectively. At the same time the drying rate in the center (position 1) starts to decrease. The center of the film dries in a shorter time as a result of a lower initial film thickness. This will stop the horizontal drying front. Figure 13b shows that for the investigated film inhomogeneous drying is observed up to position 4, that is, the drying front moves 8 mm into the film.

Coating Stability and Redispersion

For many applications it is necessary that the final coating cannot be redispersed or pentrated again by water to protect

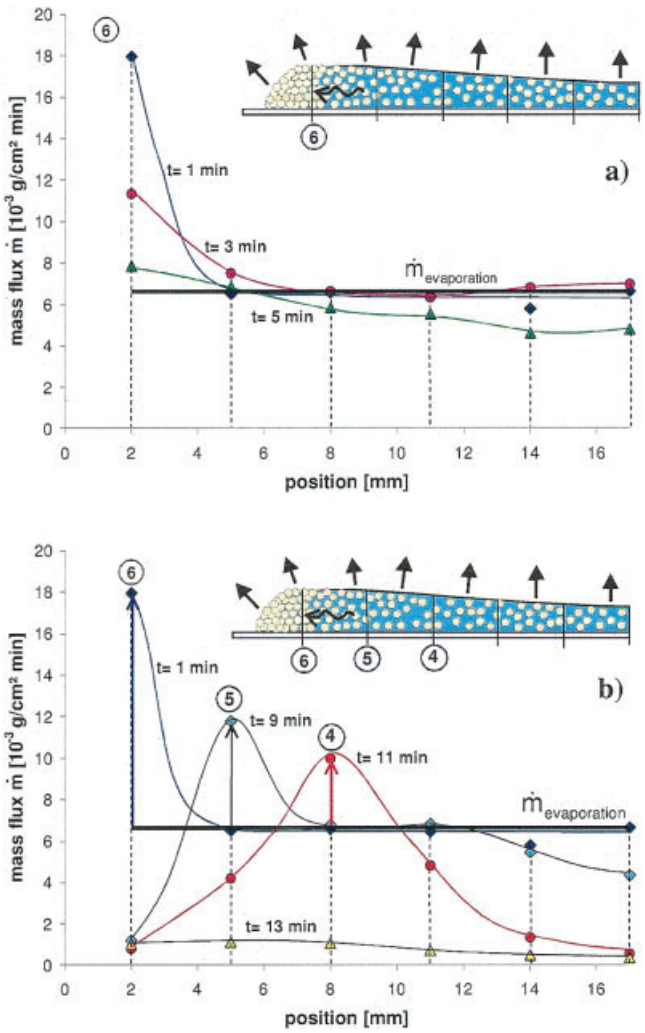

Figure 13. Mass flux at different positions across the latex film (positions 1–6) during drying.

The lines are intended only to guide the eye. (a) The higher flux at the edge of the film (position 6) is a combination of water evaporation and horizontal flux of water and particles, driven by a capillary pressure difference. Once the capillary pressure can no longer ensure horizontal flux to the film surface, a water front will recede into the film ($t = 5$ min). (b) When the water front passes by a measurement position, this is connected with an increase in the mass flux at that position. This can be observed at positions 4 and 5 for $t = 9$ min and $t = 11$ min of drying. Before the film is completely dry, the water front has moved a distance of 8 mm into the film. [Color figure can be viewed in the online issue, which is available at www.interscience.wiley.com]

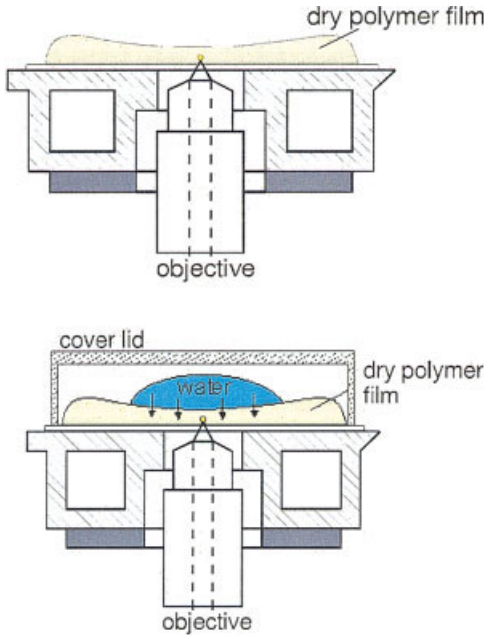

Figure 14. Representation of a redispersion experiment.

A dry latex film is scanned once to obtain its initial film thickness. Then, water is applied onto the top of the dry film and the water diffusion into the film is monitored using IMRS. [Color figure can be viewed in the online issue, which is available at www.interscience.wiley.com]

the underlaying substrate. Good film formation requires that the initial dispersion of polymer particles in water transforms into a smooth and crack-free polymer film. During film formation, the interparticular repulsive forces, initially present to stabilize the dispersion, have to be overcome. Particle deformation depends on the particle's glass-transition temperature (T_g). Incomplete film formation is the result of insufficient particle deformation and polymer interdiffusion.

In this study we set out to monitor the amount of water uptake of 1-day-old latex coatings and to correlate the findings with the film structure. Here, water diffusion into the film is tested using IMRS. For so-called redispersion experiments a large amount of water is applied onto the top of the dry polymer film (Figure 14). Depth scans through the film show the water uptake within the film and the formation of concentration profiles, respectively.

The first sample (sample I) is a 1-day-old coating of the acrylic latex dried at temperatures close to the T_{mff}. The second film, later referred to as sample II, consists of the same latex to which 4 wt % of the coalescing aid (2,2,4-trimethyl-1,3-pentandiol-monoisobutyrate) were given to facilitate deformation and polymer interdiffusion arising from its lower T_{mff}.

According to the general film-formation mechanism (Figure 1), the formation of a nonporous coating is possible for films only well above their T_{mff}. Therefore, for sample I dried at temperatures close to the T_{mff} it is expected that particle deformation will not be space filling. Then, according to the mechanism (Figure 1) individual particles will persist in the film, separated by a layer of surface-active hydrophilic material located at the particle interfaces.

Figure 15 shows the water content within the polymer film of sample I. In the figure the substrate, a glass plate, is on the left-hand side and the free surface of the polymer film on the right-hand side. The dry film has an initial thickness of $d = 67$ μm. Soon after water is applied onto the dry film, concentration profiles form (Figure 15) and, simultaneously, the film thickness increases. Swelling is possible only if the distance between the particle centers increases. A change of particle distance can occur only when intruding water reverses particle–particle contact or when the hydrophilic particle surface will lead to an increased particle diameter from the contact with water. In this experiment, the final amount of water in the film does not exceed a value of $X = 0.25$ g water/g polymer, which means that particle contact in the film is irreversible and therefore redispersion is not possible. Instead, water diffuses through the film and accumulates at the film–substrate interface. The film finally loses contact with the glass substrate. To support the above findings, AFM measurements of the film surface (Figure 15, top) show undeformed single particles and a rough and porous surface.

Addition of a hydrophobic film-formation aid to the acrylic latex dispersion lowers the T_{mff}, which enables complete particle deformation into a space-filling structure and the forma-

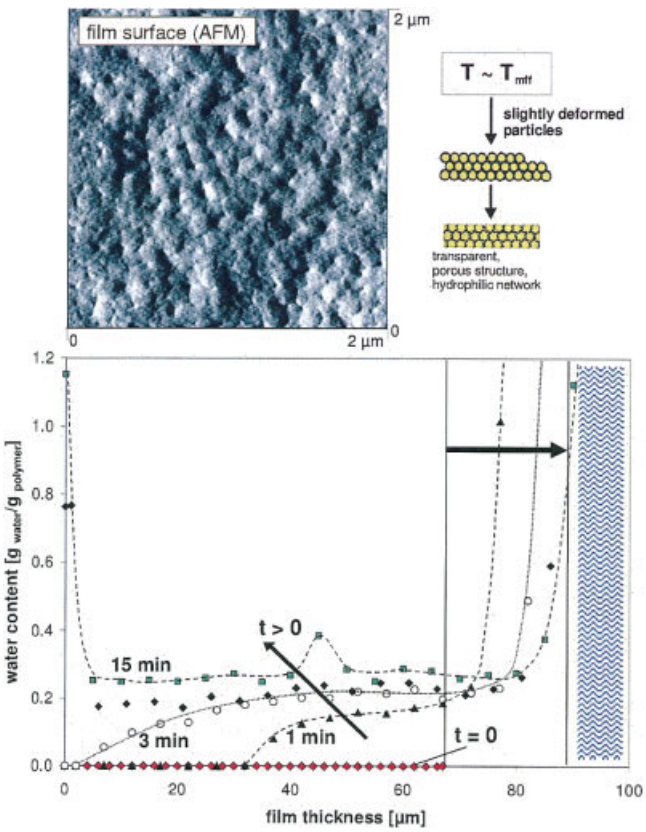

Figure 15. Redispersion experiment of a film that has been prepared at conditions close to its T_{mff} (sample I).

A dispersion of acrylic latex of high glass-transition temperature forms a rough and incomplete film. The AFM picture of the film surface shows individual particles. [Color figure can be viewed in the online issue, which is available at www.interscience.wiley.com]

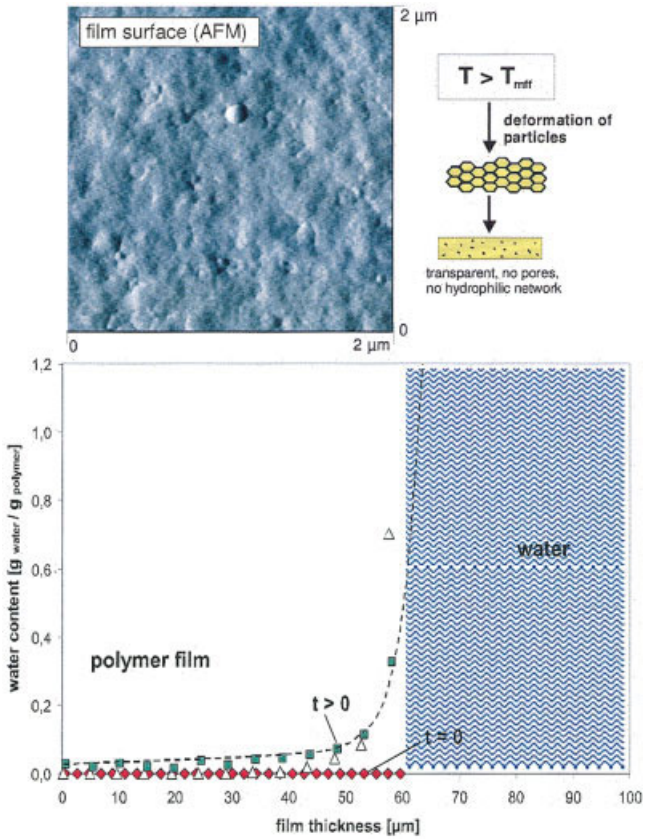

Figure 16. Redispersion experiment after the T_{mff} of the same acrylic latex dispersion has been lowered using a film-formation additive (sample II).

Better particle deformation results in a nonporous structure, which becomes visible from the AFM picture and from almost no water uptake in the film (IMRS measurement). [Color figure can be viewed in the online issue, which is available at www.interscience.wiley.com]

tion of a nonporous film. Then, particle interfaces vanish as a result of the sufficiently fast polymer interdiffusion, which destroys the network of hydrophilic surface-active material formerly present at the particle–particle interfaces. Figure 16 shows the redispersion experiment of sample II. In a comparison of the water uptake of the two formulations with and without coalescing aid, one observes there is almost no water intrusion and no swelling of the film when the additive is present. All interstitials between the particles must be closed and a penetration network of hydrophilic surface material must be interrupted by polymer chain diffusion. The AFM measurement of the film surface (Figure 16, top) shows a smooth surface of strongly deformed particles. No pores are visible, although polymer interdiffusion still seems not to be completed.

Conclusion

In contrast to solvent-based coatings most of the drying of films cast from aqueous acrylic polymer dispersion is in the constant rate period. For ambient drying conditions and a water content above $X \simeq 0.05$ g water/g polymer no concentration gradients form in the film's vertical direction. For the last scan through the film a decrease in drying rate indicates the formation of a film-side diffusion resistance. This is possibly attributable to a layer of completely deformed particles near the film surface, which forms a diffusion barrier for the remaining water in the film. A comparison of experimental data with calculated values using the constant-rate model shows very good agreement. Our observations are in accordance with the theoretical[37,38] and with the few experimental findings given in the literature.[20] IMRS is an excellent tool to obtain high-accuracy data in the film's vertical direction. An experimental study of the formation of concentration gradients toward the end of drying using IMRS would possibly give further valuable results.

In attempts to achieve further improvements in the application properties of latex formulations, industry has a fundamental interest in how to influence lateral inhomogeneous drying of films from water-based latex dispersions. Here, horizontal inhomogeneous drying was measured at six different positions within the film. The IMRS data show that the initial film thickness is nonuniform, whereas the initial water content is constant across the film. The film is thicker toward the edge as a result of the high contact angle that forms with the glass substrate.

The film's profile has a profound influence on the water content in the film during drying. Drying starts at the edge because of the greater evaporation area. In the center a higher decrease of water content is the result of lower film thickness. In accordance with the literature, the existence of a horizontal flux of water and particles arising from capillary pressure that forms from the menisci between the close packed particles was observed at the position closest to the edge (Figure 10; position 6). Horizontal flow of water within the zone of packed particles was also measured at two other positions (Figure 10; positions 4 and 5). The experimental data give a good impression about the distance over which capillary suction is effective and the final position of the drying front in the film. The strong decrease of water content resulting from horizontal flow is coupled with a strong decrease in film thickness. For the packed region (Figures 10 and 12; positions 4 and 5) this means that capillary suction causes particle deformation. Here, an investigation of formulations of different T_{mff} values would be of great importance.

Coating properties and film formation depend on the drying temperature. Many experimental studies prove that complete particle deformation takes place for drying only well above the polymer's minimum film-formation temperature (T_{mff}), whereas at temperatures close to T_{mff} the film structure is incomplete with surface-active material still present at the particle–particle interfaces. Redissolution experiments of 1-day-old films and AFM measurements of the film surface could prove this theory. For drying close to the T_{mff} strong water concentration gradients form and water accumulates at the film–substrate interface. Within the film, all particle interstitials are filled with water. The increase in film thickness is mainly the result of particle swelling after the hydrophilic material located at the particle surface has come into contact with water. Because the water content of the film does not increase above a certain value lower than that of the initial dispersion, particle contact in the film is irreversible. For films dried well above T_{mff} the particles form a

space-filling structure. IMRS redissolution experiments showed no water intrusion and no swelling of the film, which would indicate the existence of a network of hydrophilic surface-active material. The AFM picture of the film surface showed no pores. In this work the T_{mff} of the original acrylic latex dispersion was lowered by the addition of 4 wt % of a coalescing aid. By that we could change the film properties and still work at the same drying conditions. The change of T_{mff} by the addition of a small amount of coalescing aid is a good means to design film properties in the desired way. The measurement technique of IMRS used in this work provides an excellent tool to investigate and control various film-formation properties.

In the future we plan to conduct a systematic study on the inhomogeneous drying of different latex formulations. Experimental data will be compared with model calculations using the model first developed by Routh and Russel as a basis.

Notation

c_i = concentration, g/m^3
C = detector efficiency
$d_{film,end}$ = thickness of the dry polymer film, μm
d_{start} = initial film thickness, μm
D_0 = Stokes–Einstein diffusion coefficient, m^2/s
$\dot{E}$ = initial surface velocity, m/s
F = area of detector hole, m^2
I_0 = incident laser power, W/m^2
I_i = intensity, W/m^2
k = Boltzmann constant, J/K
K_S = Stefan correction term
L = length of polymer film, m
$\dot{m}_{water}$ = specific mass flow, kg/(m^{2}s)
M_i = molar mass, g/mol
N_A = Avogadro constant, 1/mol
$\dot{n}_i$ = molar flux, mol/(m^{2}s)
p = total pressure, bar
p_i = saturation pressure of i, bar
R_0 = particle diameter, nm
r_{pore} = pore radius, m
V = observation volume, m^3
x = mass fraction of polymer (initial dispersion), kg/kg
X = water content, kg/kg
$\tilde{y}^{\infty}$ = molar fraction of water in air
$\tilde{y}^*$ = molar fraction of water at the interface

Greek letters

$\beta_{g,w}$ = mass-transfer coefficient, m/s
δ_w = diffusion coefficient, m^2/s
φ = relative air humidity
μ = dynamic viscosity, Pa•s
ν = kinematic viscosity, m^2/s
ρ_{gas} = air density, kg/m^3
ρ_{H_2O} = density of water, kg/m^3
$\rho_{polymer}$ = polymer density, kg/m^3
Ω_{obs} = spatial angle, rad
$\partial\sigma_i/\partial\Omega$ = differential scattering cross section, m^2/rad

Acknowledgments

We thank Rhodia Recherches et Technologies (Aubervilliers, France) for generously financing this project and for their interest and support of this work!

Literature Cited

1. Keddie JL. Film formation of latex: A review. *Mater Sci Eng Reports*. 1997;21:101–170.
2. Winnik MA. Latex film formation. *Curr Opin Colloid Interface Sci*. 1997;2:192–199.
3. Steward PA, Hearn J, Wilkinson MC. An overview of polymer latex film formation and properties. *Adv Colloid Interface Sci*. 2000;86: 195–267.
4. Joanicot M, Wong K, Maquet J, Chevalier Y, Pichot C, Graillet C, Lindner P, Rios L, Cabane B. Ordering of latex particles during film formation. *Prog Colloid Polym Sci*. 1990;81:175–183.
5. Chevalier Y. Small-angle neutron scattering for studying latex film structure. *Trends Polym Sci*. 1996;4:197–203.
6. Joanicot M, Wong K, Richard J, Maquet J, Cabane B. Ripening of cellular latex films. *Macromoelcules*. 1993;26:3168–3175.
7. Chevalier Y, Hidalgo M, Cavaille JY, Cabane B. Structure of waterborne organic composite coatings. *Macromolecules*. 1999;32:7887–7896.
8. Belaroui F, Cabane B, Dorget M, Grohens Y, Marie P, Holl Y. Small-angle neutron scattering study of particle coalescence and SDS desorption during film formation from carboxylated acrylic latices. *J Colloid Interface Sci*. 2003;262:409–417.
9. van Tent A, te Nijenhuis K. The film formation of polymer particles in drying thin films of aqueous acrylic latices. II. Coalescence, studied with transmission spectrophotometry. *J Colloid Interface Sci*. 2000;232:350–363.
10. Kim HB, Winnik MA. Factors affecting interdiffusion rates in films prepared from latex particles with a surface rich in acid groups and their salts. *Macromolecules*. 1995;28:2033–2041.
11. Niu M, Urban MW. Recent advances in stratification and film formation of latex films; attenuated total reflection and step-scan photoacoustic FTIR spectroscopic studies. *J Appl Polym Sci*. 1998;70: 1321–1348.
12. Zhao CL, Holl Y, Pith T, Lambla M. FTIR-ATR spectroscopic determination of the distribution of surfactants in latex films. *Colloid Polym Sci*. 1987;265:823–829.
13. Richard J, Maquet J. Dynamic micromechanical investigations into particle/particle interfaces in latex films. *Polymer*. 1992;33:4164–4173.
14. Ma Y, Davis HT, Scriven LE. Microstructure development in drying latex coatings. *Prog Org Coat*. 2005;52:46–62.
15. Mallegol J, Dupont O, Keddie JL. Obtaining and interpreting images of waterborne acrylic pressure-sensitive adhesives by tapping-mode atomic force microscopy. *Langmuir*. 2001;17:7022–7031.
16. Belaroui F, Grohens Y, Boyer H, Holl Y. Depth profiling of small molecules in dry latex films by confocal Raman spectroscopy. *Polymer*. 2000;41:7641–7645.
17. Belaroui F, Hirn MP, Grohens Y, Marie P, Holl Y. Distribution of water-soluble and surface-active low-molecular-weight species in acrylic latex films. *J Colloid Interface Sci*. 2003;261:336–348.
18. Dobler F, Pith T, Lambla M, Holl Y. Coalescence mechanisms of polymer colloids. I. Coalescence under the influence of particle–water interfacial tension. *J Colloid Interface Sci*. 1992;152:1–11.
19. Rottstegge J, Traub B, Wilhelm M, Landfester K, Heldmann C, Spiess HW. Investigations on the film-formation process of latex dispersions by solid-state NMR spectroscopy. *Macromol Chem Phys*. 2003; 204:787–802.
20. Gorce JP, Bovey D, McDonald PJ, Palasz P, Taylor D, Keddie JL. Vertical water distribution during the drying of polymer films cast from aqueous emulsions. *Eur Phys J E*. 2002;8:421–429.
21. Ciampi E, Goerke U, Keddie JL, McDonald PJ. Lateral transport of water during drying of alkyd emulsions. *Langmuir*. 2000;16:1057–1065.
22. Brown GL. Formation of films from polymer dispersions. *J Polym Sci*. 1956;22:423–434.
23. Dillon RE, Matheson LA, Bradford EB. Sintering of synthetic latex particles. *J Colloid Sci*. 1951;6:108–117.
24. Sheetz DP. Formation of films by drying of latex. *J Appl Polym Sci*. 1965;9:3759–3773.
25. Routh AF, Russel WB. A process model for latex film formation: Limiting regimes for individual driving forces. *Langmuir*. 1999;15: 7762–7773.
26. Toussaint A, De Wilde M. A comprehensive model of sintering and coalescence of unpigmented latexes. *Prog Org Coat*. 1997;30:113–126.

27. Schabel W, Scharfer P, Müller M, Ludwig I, Kind M. Concentration profile measurements in polymeric coatings during drying by means of Inverse-Micro-Raman-Spectroscopy (IMRS): Raman Update Autumn 2005. *Edison, NJ: HORIBA Jobin Yvon;* 2005;3:1–3.
28. Schabel W, Scharfer P, Müller M, Ludwig I, Kind M. Messung und Simulation von Konzentrationsprofilen bei der Trocknung binärer Polymerlösungen. *Chemie Ingenieur Technik*. 2003;75:1336–1344.
29. Schabel W, Ludwig I, Kind M. Measurements of concentration profiles in polymeric solvent coatings by means of an Inverse-Confocal-Micro-Raman-spectrometer—Initial results. *Drying Technol*. 2003; 22:285–294.
30. Schabel W. Inverse Mikro Raman Spektroskopie—eine neue Messmethode zur Untersuchung lokaler Stofftransportvorgänge in dünnen Filmen, Folien und Membranen. *Chemie Ingenieur Technik*. 2005; 77:1915–1926.
31. Routh AF, Russel WB. Deformation mechanisms during latex film formation: Experimental evidence. *Ind Eng Chem Res*. 2001;40: 4302–4308.
32. Routh AF, Zimmerman WB. Distribution of particles during solvent evaporation from films. *Chem Eng Sci*. 2004;59:2961–2968.
33. Schlünder EU. Einführung in die Stoffübertragung. Braunschweig, Germany:Friedrich Vieweg & Sohn; 1996;86.
34. Gnielinski V.Wärmeübertragung bei der Strömung längs einer ebenen Wand. In:VDI-Wärmeatlas. 10th Edition. Berlin:Springer-Verlag; 2005:Gd1.
35. Lucas K, Luckas M. Berechnungsmethoden für Stoffeigenschaften. In: VDI-Wärmeatlas. 10th Edition. Berlin: Springer-Verlag; 2005: Da35.
36. Denkov ND, Velev OD, Kralchevsky PA, Ivanov IB, Yoshimura H, Nagayama K. Mechanism of formation of two-dimensional crystals from latex particles on substrates. *Langmuir*. 1992;8:3183–3190.
37. Routh A, Russel W. Horizontal drying fronts during solvent evaporation from latex films. *AIChE J*. 1998;44:2088–2098.
38. Routh A, Russel W. Process model for latex film formation: Optical clarity fronts. *J Coat Technol*. 2001;73:41–48.
39. Salamanca JM, Ciampi E, Faux DA, Glover PM, McDonald PJ, Routh AF, Peters ACIA, Satguru R, Keddie JL. Lateral drying in thick films of waterborne colloidal particles. *Langmuir*. 2001;17: 3202–3207.
40. Tirumkudulu MS, Russel W. Role of capillary stresses in film formation. *Langmuir*. 2004;20:2947–2961.

Manuscript received Mar. 30, 2006, revision received Oct. 29, 2006, and final revision received Dec. 12, 2006.